Am J Physiol Endocrinol Metab 315: E496–E510, 2018.
First published May 15, 2018; doi:10.1152/ajpendo.00061.2018.

RESEARCH ARTICLE | *Role of Gut Microbiota, Gut-Brain and Gut Liver Axes in Physiological Regulation of Inflammation, Energy Balance, and Metabolism*

Acetyl-CoA from inflammation-induced fatty acids oxidation promotes hepatic malate-aspartate shuttle activity and glycolysis

Tongxin Wang, Weilei Yao, Ji Li, Qiongyu He, Yafei Shao, and Feiruo Huang

Department of Animal Nutrition and Feed Science, College of Animal Science and Technology, Huazhong Agricultural University, Wuhan, China

Submitted 15 February 2018; accepted in final form 2 April 2018

Wang T, Yao W, Li J, He Q, Shao Y, Huang F. Acetyl-CoA from inflammation-induced fatty acids oxidation promotes hepatic malate-aspartate shuttle activity and glycolysis. *Am J Physiol Endocrinol Metab* 315: E496–E510, 2018. First published May 15, 2018; doi:10.1152/ajpendo.00061.2018.—Hepatic metabolic syndrome is associated with inflammation, as inflammation stimulates the reprogramming of nutrient metabolism and hepatic mitochondria-generated acetyl-CoA, but how acetyl-CoA affects the reprogramming of nutrient metabolism, especially glucose and fatty acids, in the condition of inflammation is still unclear. Here, we used an acute inflammation model in which pigs were injected with lipopolysaccharide (LPS) and found that hepatic glycolysis and fatty acid oxidation are both promoted. Acetyl-proteome profiling of LPS-infected pigs liver showed that inflammatory stress exacerbates the acetylation of mitochondrial proteins. Both mitochondrial glutamate oxaloacetate transaminase 2 (GOT2) and malate dehydrogenase 2 (MDH2) were acetylated, and the malate-aspartate shuttle (MAS) activity was stimulated to maintain glycolysis. With the use of ^{13}C-carbon tracing in vitro, acetyl-CoA was found to be mainly supplied by lipid-derived fatty acid oxidation rather than glucose-derived pyruvate oxidative decarboxylation, while glucose was mainly used for lactate production in response to inflammatory stress. The results of the mitochondrial experiment showed that acetyl-CoA directly increases MDH2 and, in turn, the GOT2 acetylation level affects MAS activity. Treatment with palmitate in primary hepatocytes from LPS-injected pigs increased the hepatic production of acetyl-CoA, pyruvate, and lactate; MAS activity; and hepatic MDH2 and GOT2 hyperacetylation, while the deficiency of long-chain acetyl-CoA dehydrogenase resulted in the stabilization of these parameters. These observations suggest that acetyl-CoA produced by fatty acid oxidation promotes MAS activity and glycolysis via nonenzymatic acetylation during the inflammatory stress response.

acetyl-CoA; fatty acid oxidation; glycolysis; inflammation; malate-aspartate shuttle

INTRODUCTION

The increasing incidences of obesity, type 2 diabetes mellitus (T2DM), and other chronic metabolic diseases are prevalent health problems worldwide (8). The occurrence of metabolic syndromes is known to be closely associated with inflammatory stress (54). The liver is the central organ that plays major metabolic roles in regulating the homeostasis of glucose, lipids, and amino acids during alterations of metabolic conditions (4, 34). In response to inflammation, the metabolism may switch from carbohydrate utilization and lipogenesis to fatty acid oxidation (34). In addition, hepatic mitochondrial performance, which integrates the metabolic networks needed to maintain bioenergetic requirements, steadily decays as part of the many adverse outcomes of chronic energy imbalance (29). Deregulation of mitochondrial metabolic networks can lead to mitochondrial dysfunction, a common condition in many diseases. Accordingly, disease-associated perturbations in liver mitochondrial quality and function have broad-ranging clinical and therapeutic implications.

Recent findings using mass spectrometry (MS) have drawn attention to lysine acetylation as a prominent mitochondrial posttranslational modification (PTM), which is now increasingly recognized as a marker of cellular energy stress (11, 17, 23, 47, 49). Altered mitochondrial acetylation has been associated with various diseases, including cardiovascular disease, cancer, aging, metabolic disorders, and inflammation (2, 3, 9, 25). SIRT3 catalyzes protein deacetylation (17, 38, 47); however, the involvement of liver mitochondrial acetylation in this process remains unclear, especially during disease. An emerging theory suggests that acetylation of mitochondrial proteins occurs largely through nonenzymatic mechanisms. Recent studies provided models to predict that physiological and nutritional conditions that raise mitochondrial concentrations of acetyl-CoA "push" protein acetylation by expanding the local pool of acetyl donors. These findings imply that reversible posttranslational protein acetylation modifications are emerging as critical regulators of mitochondrial function and form a direct link between metabolism and protein function via the metabolic intermediate acetyl-CoA (10, 15, 33, 51).

As a growing number of studies suggest that reprogramming nutrient metabolism plays a central role in inflammation (6, 39, 53, 55), liver mitochondrial acetyl-CoA and nonenzymatic acetylation may be the key factors that regulate this mechanism during the inflammatory stress response. Under normal conditions, the mitochondrial pool of acetyl-CoA is mainly supplied by glucose-derived pyruvate oxidative decarboxylation and lipid-derived fatty acid oxidation; however, little is known about whether both of these processes occur simultaneously or one is a dominant pathway to generate acetyl-CoA during inflammation. In recent studies, inflammation-induced lipolysis was found to directly lead to an increased hepatic acetyl-

Address for reprint requests and other correspondence: F. Huang, Dept. of Animal Nutrition and Feed Science, College of Animal Science and Technology, Huazhong Agricultural Univ., Wuhan 430070, China (e-mail: huangfeiruo@mail.hzau.edu.cn).

CoA content (41). Additionally, fatty acid oxidation was found to reprogram cellular metabolism, leading to an increase in lipid-derived acetyl-CoA and inhibition of glucose breakdown in the TCA cycle (19). Then, there is a serious possibility that the generation of acetyl-CoA may not depend on glucose-derived pyruvate oxidative decarboxylation during inflammation. In such a case, the question remains as to the metabolic fate of glucose during inflammation. Of note, an important phenomenon is steadily emerging from studies examining inflammatory stress, especially in immunocytes, such that glycolysis would be enhanced and glucose would be converted to lactate rather than acetyl-CoA, even under normoxic conditions (24, 58). However, whether this phenomenon occurs in liver/hepatocyte is still unclear. A high glycolytic rate is known to lead to much higher levels of cytosolic NADH/NAD^+ ratios that may in turn inhibit glycolysis (52). In this case, the malate-aspartate shuttle (MAS), one of the NADH shuttles, may play a significant role in maintaining glycolysis, as it is widely accepted that the major function of NADH shuttles is to mediate the transfer of the reducing equivalents of cytosolic NADH into mitochondria (52). Hence, we hypothesized that increased hepatic acetyl-CoA due to fatty acid oxidation is responsible for increasing MAS activity and glycolysis via nonenzymatic acetylation during the inflammatory stress response.

The first goal of the present study was to investigate the dynamics of mitochondrial lysine acetylation in the liver of pigs and to elucidate the mechanism of fatty acid oxidation-induced hepatic mitochondrial acetylation in response to inflammatory stress. Additionally, this study aimed to reveal the relevance between hepatic glycolysis and fatty acid oxidation-induced mitochondrial protein acetylation in the response to inflammatory stress. A TMT-labeling quantitative MS-based acetyl-proteomics approach was used to examine hepatic acetylation in response to lipopolysaccharides (LPS) infection, and this study provides several lines of evidence in vivo and in vitro that acetyl-CoA produced from fatty acid oxidation promotes hepatic mitochondrial MAS activity and glycolysis via nonenzymatic acetylation during the inflammatory stress response.

MATERIALS AND METHODS

Animals experiments. The animal handling protocol followed in the current study was approved by the Animal Care and Use Committee of College of Animal Sciences and Technology, Huazhong Agricultural University and was in compliance with the National Research Council's *Guide for the Care and Use of Laboratory Animals*. The Hubei Jinlin animal company approved the animal studies. Twelve castrated Duroc × Landrace × Yorkshire pigs weighing ~30 kg were individually housed in 1.5 × 0.75 m metabolic cages in a temperature-controlled room at 21–25°C. After the pigs acclimated for at least 1 wk, the pigs were in apparent good health and then randomly divided into two groups ($n = 6$): LPS (treat) and phosphate-buffered saline (PBS; control) group. Pigs were injected intraperitoneally with LPS (from *Escherichia coli* 055:B5; Sigma) at 100 μg/kg body wt or equivalent PBS. The animals were euthanized 7 h after administration. Blood samples were collected from pigs precaval vein (per hour) and hepatic vein (after animals euthanized). Liver tissue and blood were collected and stored at −80°C until needed for bioassays.

Cell culture. HEK293T cells and Chang's liver cells were cultured in DMEM media supplemented with 10% new born bovine serum (Biochrom, Berlin, Germany) (59). HEK293T cells and Chang's liver cells were incubated according to the protocols described below. Hepatocytes were isolated from LPS-treated livers of pigs by collagenase perfusion and mechanical disruption (16). Cell viability (assessed by Trypan blue exclusion) was >90%. Hepatocytes were plated onto collagen-coated glass plates at 1.9×10^4 cells/cm^2 in DMEM medium supplemented with 10% fetal bovine serum (Sigma), penicillin (100 U/ml), and streptomycin (100 μg/ml; Invitrogen, San Diego, CA). Cells were incubated at 37°C in a humidified atmosphere with 5% CO_2 for 3 h, allowing cell attachment to plates. After that time, the medium was changed, and hepatocytes were incubated according to the protocols described below. At the end of the experiments, cells were washed and sonicated in 0.3 M sucrose (Merck Chemicals, Darmstadt, Germany) (48).

Metabolomic profiling. Hepatocytes were plated at 2×10^6 cells per 10-cm dish and allowed to seed overnight. The following day cells were treated with DMEM + 10% FBS containing either PBS or 2 mM palmitate for 24 h. After 24 h, cells were washed with ice-cold PBS, scraped from plates in ice cold PBS and then spun down in a swinging bucketed centrifuge at 500 *g* for 5 min to pellet cells at 4°C. Cell pellets were then lysed in 300 μl 0.6% formic acid, and 30 μl were then removed for protein quantification, followed by addition of 270 μl acetonitrile to give a final concentration of 0.3% formic acid and 50% acetonitrile. Organic acids were analyzed using stable isotope dilution technique. Organic acids were quantified using methods described previously (21) employing Trace Ultra GC coupled to ISQ MS operating under Xcalibur 2.2 (Thermo Fisher Scientific, Austin, TX).

Isotope tracer experiments and gas chromatography-mass spectrometry analysis. For isotope tracing experiments, hepatocytes were seeded in six-well dishes and harvested as described above. Metabolic steady state was determined from cells collected at 2, 6, 12, and 24 h posttreatment. Cells were washed and scraped with PBS on ice. Pellets and collected media were stored at −80°C. Gas chromatography-mass spectrometry (GC-MS) analysis was performed on an Agilent 7890B GC system equipped with a HP-5MS capillary column (30 m, 0.25-mm inner diameter, 0.25-μm phase thickness; Agilent J&W Scientific), connected to an Agilent 5977A Mass Spectrometer operating under ionization by electron impact at 70 eV. Helium flow was maintained at 1 ml/min. The source temperature was maintained at 230°C, the MS quad temperature at 150°C, the interface temperature at 280°C, and the inlet temperature at 250°C (intracellular metabolites and glucose). Mass spectra were recorded in selected ion monitoring mode with 4-ms dwell time. ^{13}C labeling of a metabolite was determined as previously described (26), In brief, ^{13}C labeling = $1/n \sum_{i=1}^{n} i(M + i)$, where n is the number of carbon atoms in a given MS fragment and $M + i$ are the relative mass isotopomer abundances after correction for natural isotope abundances.

Intracellular metabolite derivatization and ^{13}C assay. Harvested metabolite samples were allowed to thaw, and 750 μl methanol were added to each sample. Samples were briefly vortexed before centrifugation at 14,000 *g* for 10 min. Protein-free supernatants were transferred and evaporated to dryness under N_2 gas-flow at 37°C using an evaporator. Tert-butyldimethylsilyl (TBDMS)-derivatized metabolites were performed as described in Ref. 1 with slight modifications. Briefly, metabolites were resuspended in 25 μl of methoxylamine hydrochloride [2% (wt/vol) in pyridine] and incubated at 40°C for 90 min on a heating block. After brief centrifugation, 35 μl of MTBSTFA + 1% TBDMS were added and the samples were incubated at 60°C for 30 min. The derivatized samples were centrifuged for 5 min at 14,000 *g*, and the supernatants were transferred to GC vials for GC-MS analysis. The injection volume was 1 μl, and samples were injected in split or splitless mode depending on analyte of interest. GC oven temperature was held at 80°C for 2 min, increased to 280°C at 7°C/min, and held at 280°C for a total run time of 40 min. [^{13}C]acetyl-CoA was analyzed using a method published by Magnes et al. (30). The acetyl-CoA was further purified by solid phase extraction (37).

The acetyl-CoA was measured by flow injection analysis using positive electrospray ionization on Xevo TQ-S, a triple quadrupole mass spectrometer (Waters, Milford, MA) employing methanol/water (80/20, vol/vol) containing 30 mM ammonium hydroxide as the mobile phase. Spectra were acquired in the multichannel acquisition mode monitoring the neutral loss of 507 Da.

Radiolabeled oxidation assays. Hepatocytes were plated at 80,000 cells per well in 24-well plates and treated the next day with 2 mM palmitate or PBS in complete media with 10% FBS. Twenty-four hours later media were removed and replaced with media containing ^{14}C-labeled substrate for 1.5 h. Palmitate was not present during the oxidation period. After 1.5 h, the media were collected and added to a NaOH trap to capture CO_2. The trap was set up with medium collected from well placed at the bottom of a glass tube, which had a smaller tube elevated inside of it that contained NaOH. The trap was capped with a rubber septa, and perchloric acid was added via syringe to the bottom of the trap to promote the release of CO_2. Traps were then placed on a shaker for 1 h, after which the NaOH fraction was collected and added to scintillation vials, and ^{14}C radioactivity was measured with a scintillation counter. Decays per minute were normalized to protein content determined by bicinchoninic acid assay (BCA) solution (cat. no. B9643; Sigma) and copper(II) sulfate solution (cat. no. 2284; Sigma).

HEK293T and Chang's liver cells treatment and transient transfection. Tricostatin A (TSA) treatment was carried out by adding 10 μM TSA to the culture medium 16–20 h before harvest cells, Nicotinamide treatment was carried out by addition of 5–10 mM nicotinamide to the culture medium 4–8 h before harvest cells as previously described (59). The cDNA encoding glutamate oxaloacetate transaminase 2 (GOT2) and malate dehydrogenase 2 (MDH2) were cloned into Flag, Myc (pcDNA-Flag; pcDNA-Myc). Point mutations of GOT2 and MDH2 were generated by QuickChange Site-Directed Mutagenesis kit (Stratagene) (57). Plasmid transfection was carried out either by calcium phosphate method for HEK293T or Lipofectamine 2000 (Invitrogen) for Chang's liver cells (59).

Long-chain fatty acid desaturase silencing, fatty acid preparation, and treatment. Primary cultured hepatocytes isolated from LPS-treated livers of pigs were transfected with long-chain fatty acid desaturase (LCAD) siRNA to silence target proteins. The hepatocytes were transfected with Lipofectamine 2000 (Invitrogen) using 150 pmol/well of the LCAD siRNAs (Santa Cruz Biotechnology). For the nonesterified fatty acid (NEFA) preparation, NEFA stock solutions were prepared by coupling free fatty acids with bovine serum albumin (BSA) (12). First, palmitate was dissolved in pure ethanol at a concentration of 195 mM so that the final concentration of ethanol in our NEFA stock solutions did not exceed 1.5% by volume. This solution was then added to a prewarmed 10% wt/wt BSA solution (37°C) to achieve a final NEFA concentration of 3 mM, and this solution was allowed to incubate in a water bath for an additional 10 min. The final ratio of NEFA to BSA was 2:1. All vehicle treatments were prepared using stocks of 10% wt/wt BSA with an equivalent volume of ethanol added to match the concentration in NEFA stocks. The final concentration of ethanol in all experimental treatments was <0.2% by volume. Hepatocytes in the absence or presence of transfection with corresponding LCAD siRNAs were treated with 200 and 400 μM palmitate described above.

Biochemical analyses and extracellular metabolite assay. The liver and hepatocyte acetyl-CoA concentration and enrichment was measured by liquid chromatography-mass spectrometry/mass spectrometry (LC-MS/MS). Serum NEFA concentrations were measured using the Biochemistry Analyzer. The serum lactate and pyruvate concentrations were determined by means of a Pierce BCA Protein Assay Kit. ELISA (Qiagen) kits were used to measure the serum concentrations of inflammatory cytokines tumor necrosis factor-α (TNF-α) and interleukin 6 (IL-6) following the manufacturer's instructions. For 3-hydroxybutyrate analysis, EDTA blood (75 μl) was directly mixed with 75 μl 1 M perchloric acid, stored on ice for at least 10 min, and frozen at −20°C until analysis of 3-hydroxybutyrate levels by LC-MS/MS. Blood glucose levels were analyzed in blood from saphenous vein using a glucometer (44). Extracellular pyruvate and lactate assay were measured by NADH-coupled lactate dehydrogenase (LDH) spectrophotometric assay and determined by means of a Pierce BCA Protein Assay Kit (52).

Preparation of mitochondrian and acetyl-CoA treatment. Mitochondria were isolated from the LPS-injected livers as well as various treated hepatocytes. First, the livers and hepatocytes were homogenized with a glass-Teflon Potter homogenizer. Mitochondria were isolated in medium containing 0.3 mmol mannitol, 10 mmol potassium HEPES (pH 7.4), and 0.2 mmol EGTA (pH 7.4) and then washed twice and suspended in the same medium without EGTA. Mitochondrial subfractionation was performed to obtain mitochondrial membrane and matrix fractions (27). For the reaction with acetyl-CoA, 0.5 mg/ml solution at pH 7.8 were treated with 1.5 mM acetyl-CoA for 5 min at room temperature.

Liver tissue and hepatocytes MAS activity. Liver and hepatocytes mitochondria were prepared as above and resuspended in 100 μl of Buffer B. The MAS assay was adapted from Contreras and Satrustegui (9a). Briefly, 100 μg of mitochondria were mixed with 10 mM pH 7.4 Tris, 300 mM mannitol, 10 mM K_2HPO_4, 5 mM $MgCl_2$, and 10 μM KCl before addition of 4 units/ml aspartate aminotransferase, 6 units/ml malate dehydrogenase, 140 μM NADH, 5 mM aspartate, and 0.5 mM ADP. Experiments were performed in a final volume of 200 μl using a black 96-well plate. Once a baseline was achieved, MAS activity was initiated by adding 5 mM glutamate and 5 mM malate and the decrease in NADH fluorescence was monitored at 340 nm (Fluostar Omega; BMG Labtech). All assays were performed at 37°C. The rate of change of florescence was expressed as nanomoles of NADH oxidized (36).

Western Blots and immunoprecipitation. Hepatic proteins were detected using antibodies against pyruvate kinase (PK), glucokinase (GK), pyruvate dehydrogenase (PDH), lactate dehydrogenase A (LDHA), LCAD, 3-hydroxyacyl CoA dehydrogenase (HADH), carnitine palmitoyltransferase (L-CPT-1), β-actin, SIRT3, and mtHSP70 (1:1,000 dilution; Abcam) (27). For immunoprecipitation, hepatocytes mitochondrial lysates were performed with anti-MDH2 or anti-GOT2 antibody (1:1,000 dilution; Abcam) overnight at 4°C and then protein A/G beads (Millipore) were added for 4 h followed by Western blotting using anti-acetyl-lysine antibody (1:1,000 dilution; Abcam). HEK293T cells were lysed in NP-40 buffer containing protease inhibitor cocktail (Roche). Immunoprecipitation was carried out either by incubating FLAG/Myc beads at 4°C with lysate for 3–4 h or by incubate appropriate antibody with cell lysate for 2–3 h, followed by incubating protein-A beads (Upstate). Standard Western blotting procedures were followed for protein and tags analysis. For acetylation Western blotting, 50 mM Tris (pH 7.5) with 10% (vol/vol) Tween-20 and 1% peptone (AMRESCO) were used for blocking and 50 mM Tris (pH 7.5) with 0.1% peptone was used to prepare primary and secondary antibodies (59).

Enzymatic activity assay. The culture supernatants were collected from treated cells at the indicated time points and stored at −80°C. The pig plasma and tissue were homogenized in DMEM and stored at −80°C. Before measurements, the plasma and tissue samples were thawed and centrifuged at 5,000 *g*, and the supernatants were collected. Enzymatic activity for LCAD was measured by the anaerobic ETF fluorescence reduction assay (13). The activity of a malate dehydrogenase was measured at 340 nm by NADH oxidation (43). The enzyme activity of GOT2 was determined by using a Glutamate-Oxaloacetate Transaminase Activity Assay Kit (Sigma) (57). LDHA activities were assayed via the consumption of NADH in the presence of pyruvate (16a). Total PDH activity was measured following incubation of extracts with PDH phosphatase and bivalent cations, and PDH activity is expressed as a percentage of the total activity (32). The HADH activity was measured according to the spectrophotometric method as previously described (5). L-CPT-1 activity was mea-

sured at 30°C and pH 7.2 according to previously described method (35). Endogenous MDH2 and GOT2 assay was carried out by substrate depletion approaches (59). In brief, substrates for a given enzyme in cell lysate were depleted by addition of an excessive amount of all other substrates except one of them. After the reaction reached equilibrium, the left out substrate was added and endogenous enzyme activity was determined.

Protein extraction (quantitative proteomics). Sample was first grinded by liquid nitrogen for 10 min and was transferred to a 5-ml centrifuge tube and sonicated three times on ice using a high-intensity ultrasonic processor (Scientz) in lysis buffer [8 M urea, 10 mM DTT, 50 mM nicotinamide (NAM), 3 μM TSA, and 0.1% protease inhibitor cocktail]. The remaining debris was removed by centrifugation at 20,000 *g* at 4°C for 10 min. The protein was precipitated with cold 15% TCA for 2 h at −20°C. After centrifugation at 4°C for 10 min, the supernatant was discarded. The remaining precipitate was washed with cold acetone for three times. The protein was redissolved in buffer (8 M urea and 100 mM TEAB, pH 8.0), and the protein concentration was determined with 2-D Quant Kit according to the manufacturer's instructions.

Trypsin digestion. For digestion, the protein solution was reduced with 10 mM DTT for 1 h at 37°C and alkylated with 20 mM IAA (Sigma) for 45 min at room temperature in darkness. For trypsin digestion, the protein sample was diluted by addition of 100 mM TEAB to a urea concentration <2 M. Finally, trypsin (Promega) was added at 1:50 trypsin-to-protein mass ratio for the first digestion overnight and 1:100 trypsin-to-protein mass ratio for a second 4-h digestion.

TMT labeling. After trypsin digestion, peptide was desalted by Strata X C18 SPE column (Phenomenex) and vacuum dried. Peptide was reconstituted in 0.5 M TEAB and processed according to the manufacturer's protocol for 6-plex TMT kit (Thermo). Briefly, one unit of TMT reagent were thawed and reconstituted in ACN (Fisher Chemical). The peptide mixtures were then incubated for 2 h at room temperature and pooled, desalted and dried by vacuum centrifugation.

Affinity enrichment. To enrich Kac peptides, tryptic peptides dissolved in NETN buffer (100 mM NaCl, 1 mM EDTA, 50 mM Tris·HCl, and 0.5% NP-40, pH 8.0) were incubated with prewashed antibody beads (PTM Biolabs) at 4°C overnight with gentle shaking. The beads were washed four times with NETN buffer and twice with ddH_2O. The bound peptides were eluted from the beads with 0.1% TFA (Sigma-Aldrich). The eluted fractions were combined and vacuum dried. The resulting peptides were cleaned with C18 ZipTips (Millipore) according to the manufacturer's instructions, followed by LC-MS/MS analysis.

LC-MS/MS analysis. Peptides were dissolved in 0.1% FA (Fluka), directly loaded onto a reversed-phase precolumn (Acclaim PepMap 100; Thermo Scientific). Peptide separation was performed using a reversed-phase analytical column (Acclaim PepMap RSLC; Thermo Scientific). The gradient comprised an increase from 3 to 22% solvent B (0.1% FA in 98% ACN) for 26 min, 22 to 35% for 8 min, and climbing to 80% in 3 min then holding at 80% for the last 3 min, all at a constant flow rate of 350 nl/min on an EASY-nLC 1000 UPLC system, the resulting peptides were analyzed by Q Exactive hybrid quadrupole-Orbitrap mass spectrometer (ThermoFisher Scientific). The peptides were subjected to NSI source followed by tandem mass spectrometry (MS/MS) in Q Exactive (Thermo) coupled online to the UPLC. Intact peptides were detected in the Orbitrap at a resolution of 70,000. Peptides were selected for MS/MS using NCE setting as 28; ion fragments were detected in the Orbitrap at a resolution of 17,500. A data-dependent procedure that alternated between 1 MS scan followed by 20 MS/MS scans was applied for the top 20 precursor ions above a threshold ion count of 5E3 in the MS survey scan with 15.0 s dynamic exclusion. The electrospray voltage applied was 2.0 kV. Automatic gain control was used to prevent overfilling of the Orbitrap; 5E4 ions were accumulated for generation of MS/MS spectra. For MS scans, the *m/z* scan range was 350–1,800. Fixed first mass was set as 100 *m/z*.

Database search. The resulting MS/MS data were processed using MaxQuant with integrated Andromeda search engine (v.1.4.1.2). Tandem mass spectra were searched against swissprot sus scrofa database concatenated with reverse decoy database. Trypsin/P was specified as cleavage enzyme allowing up to four missing cleavages, five modifications per peptide, and five charges. Mass error was set to 10 ppm for precursor ions and 0.02 Da for fragment ions. Carbamidomethylation on Cys was specified as fixed modification and oxidation on Met, and acetylation on Lys and acetylation on protein NH_2 terminal were specified as variable modifications. False discovery rate thresholds for protein, peptide, and modification site were specified at 1%. Minimum peptide length was set at 7. For quantification method, TMT-6plex was selected. All the other parameters in MaxQuant were set to default values. The site localization probability was set as >0.75.

Statistical analysis. All experiments were carried out at least three times with similar results. Analyses were conducted using Prism5 (Graph Pad Software). Results are expressed as means ± SD. Data were compared with two way ANOVA with subsequent Bonferroni post test for multiple comparisons or with Student's *t*-test. For all tests, $P < 0.05$ was considered significant.

RESULTS

Inflammatory stress promotes hepatic glycolysis and fatty acid oxidation. Pigs were given LPS injections to induce inflammatory stress and to determine the effects of LPS on the metabolic response in the liver. After treatment, the concentrations of TNF-α reached peak value at 1 h and IL-6 continuously increased until 4 h (Fig. 1, *A* and *B*), indicating that inflammatory stress had been successfully accomplished. In addition, glucose, NEFA, and lactate concentrations were tested to evaluate blood nutrient dynamics. Blood glucose levels increased slightly in the first hour and then declined rapidly in the next hour from 920 to 700 ng/ml and continued to gradually decrease through the inflammatory stress period down to 600 ng/ml (Fig. 1*D*). The levels of lactate in hepatic vein blood started to increase rapidly to peak 2,900 μmol/l in the first hour, slightly decreased to 2,700 μmol/l in the next hour, and then persisted during the period of stress (Fig. 1*E*). The levels of NEFA in plasma gradually increased during the initial 7 h and then continued to climb (Fig. 1*C*).

To further evaluate the glucose and fatty acid metabolism, a series of enzyme activity and enzyme protein amounts in glycolysis and fatty acid oxidation were tested. Seven hours after LPS injection, the enzyme activity and protein amount of GK, PK, and LDHA, which are the major regulators in glycolysis, were significantly increased in the livers of LPS-injected pigs compared with PBS-injected pigs ($P < 0.01$, Fig. 1, *H–J*). Consistent with this increased enzyme activity, significantly increased levels of hepatic vein pyruvate production were found in the LPS-injected pigs, which indicated an increase in hepatic glycolysis in response to inflammatory stress ($P < 0.001$, Fig. 1*F*), while the activity of PDH decreased ($P < 0.05$, Fig. 1, *H–J*). In addition, the activity and amount of fatty acid oxidation by the enzymes LCAD, HADH, and L-CPT-1 increased significantly, and the levels of 3-hydroxybutyrate in plasma started to increase after 30 min of LPS infusion to 247 μmol/l and further increased during the period of stress to 1000 mmol/l, indicating that liver fatty acid oxidation rate increase in response to inflammatory stress ($P < 0.05$, Fig. 1, *H–K*).

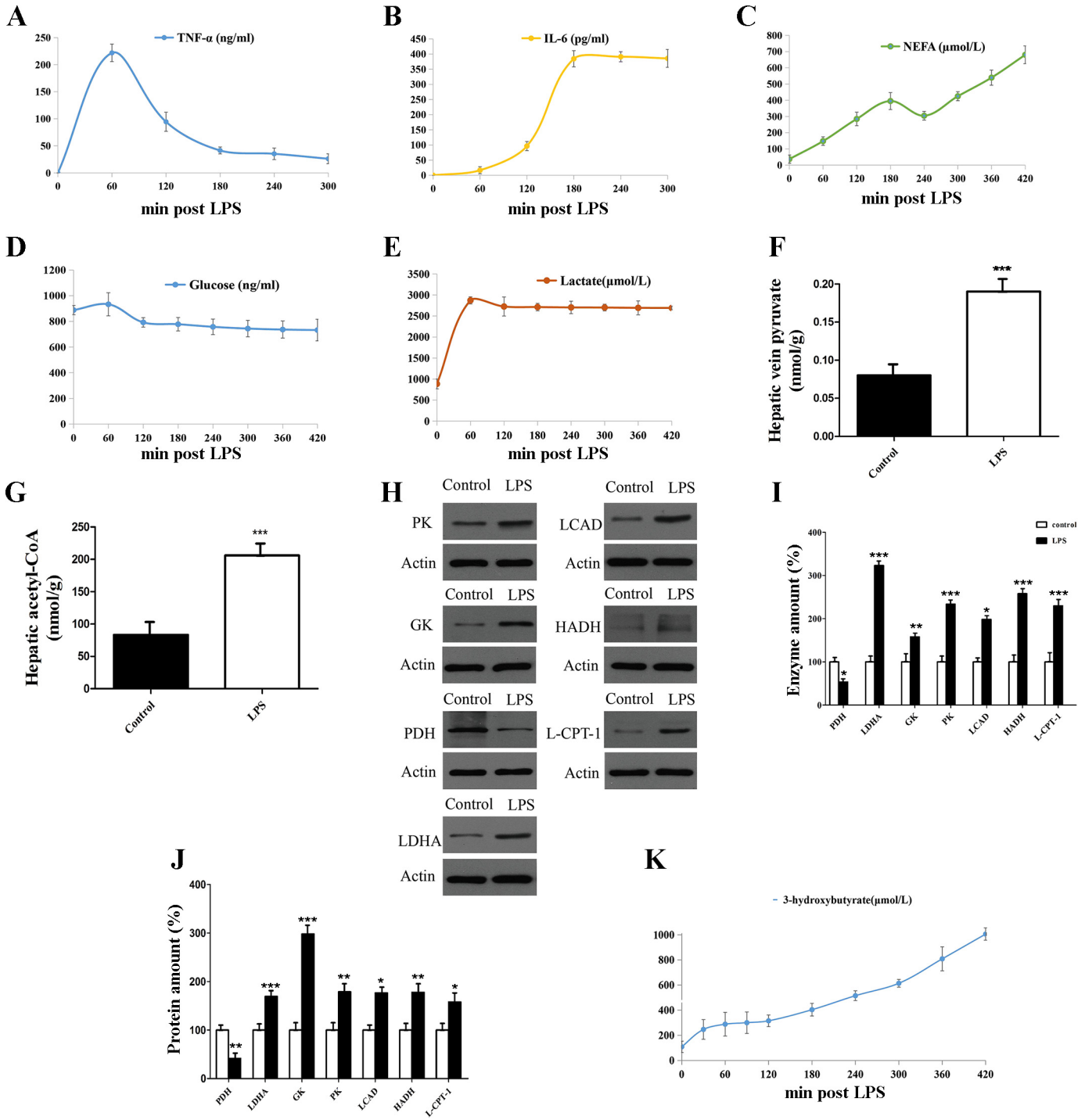

Fig. 1. LPS induces hepatic glycolysis and fatty acid oxidation. *A* and *B*: serum TNF-α concentration (ng/ml) and IL-6 concentration (pg/ml) after treatment with LPS at every hour time point. *C–E*: serum nonesterified fatty acid (NEFA; μmol/l), glucose (ng/ml), and lactate concentration (μmol/l) after treatment with LPS at every hour time point. *F–G*: hepatic vein pyruvate concentration (mmol/l) and hepatic acetyl-CoA content (nmol/g protein). *H* and *J*: pyruvate dehydrogenase (PDH), lactate dehydrogenase A (LDHA), glucokinase (GK), pyruvate kinase (PK), long-chain fatty acid desaturase (LCAD), 3-hydroxyacyl CoA dehydrogenase (HADH), and carnitine palmitoyltransferase (L-CPT-1) protein levels and enzyme activities in pigs liver. *K*: serum ketone bodies (3-hydroxybutyrate) concentration (μmol/l) after treatment with LPS at every hour time point. Blood samples were collected from pigs precaval vein/hepatic vein; control indicates PBS injection. Liver samples were collected from pigs after 7-h LPS/PBS (100 μg/kg body wt) injection. Data are means ± SD; $n = 6$. *$P < 0.05$, **$P < 0.01$, ***$P < 0.001$ from control group.

Since NEFA generated during lipolysis of adipose tissue may be critical for increasing fatty acid flux to the liver, resulting in higher hepatic acetyl-CoA concentrations (41), a novel LC-MS/MS technique was used to measure hepatic acetyl-CoA content. Predictably, the results demonstrated that LPS injection enhanced the production of hepatic acetyl-CoA compared with controls ($P < 0.001$, Fig. 1*G*), confirming fatty acid oxidation in liver mitochondria. These results suggested that

the increased glucose utilization mainly contributed to lactate production, while the increased fatty acid oxidation contributed to the generation of acetyl-CoA in response to inflammatory stress.

The accumulation of acetyl-CoA in response to inflammatory stress is mainly due to fatty acid oxidation rather than pyruvate carboxylation. The results showed that inflammatory stress promoted hepatic glycolysis and fatty acid oxidation as well as the plasma NEFA concentration. Consistent with the glucose-sparing effect known as the Randle cycle, fatty acid oxidation inhibits glucose oxidation in part by inhibiting PDH (19, 46). During inflammation, it can be predicted that increased fatty acid oxidation may be the major carbon source of acetyl-CoA, rather than pyruvate carboxylation. To test this hypothesis, this study examined the TCA cycle metabolism using targeted MS of organic acids in primary porcine hepatocytes isolated from LPS-injected pigs treated with palmitate. The results showed that pyruvate, citrate, oxaloacetate, and malate were increased, along with lactate, in palmitate-treated hepatocytes, consistent with the observations in vivo ($P < 0.05$, Fig. 2*A*). However, the oxidation of [2-^{14}C]pyruvate to $^{14}CO_2$ in palmitate-treated hepatocytes was found to be reduced compared with controls (~60%) indicating the inhibition of pyruvate oxidation ($P < 0.01$, Fig. 2*B*). Then, the isotope-labeling pattern of citrate, a central TCA cycle metabolite that can be produced from both glucose and fatty acids, was examined to further test the contribution of glucose and fatty acids to the TCA cycle in LPS-injected hepatocytes. From [U-^{13}C]glucose, the predominantly labeled isotopomer of citrate was $M + 2$, indicating that pyruvate had passed through PDH to form acetyl-CoA and condensed with unlabeled four-carbon oxaloacetate to form citrate. However, when cells were given palmitate in the presence of [U-^{13}C]glucose, the levels of $M + 2$ citrate decreased by more than 60% compared with control samples. Furthermore, $M + 4$ and $M + 5$ isotopomers, which represent further turns of glucose carbon in the TCA cycle, were almost undetectable upon palmitate treatment (Fig. 2*C*). These results indicated that fatty acid oxidation reduced the contribution of glucose to the TCA cycle in LPS-injected pig hepatocytes.

To further directly test the contribution of palmitate and glucose to the total cellular acetyl-CoA pool, LPS-injected pig hepatocytes were treated with [U-^{13}C]glucose in the presence of unlabeled 2 mM palmitate compared with [U-^{13}C]palmitate labeling in the presence of unlabeled glucose. When cells were given [U-^{13}C]glucose in the presence of palmitate, nearly 5% of the total acetyl-CoA pool was labeled; however, in cells given [U-^{13}C]palmitate, the labeling of acetyl-CoA was nearly 80% (Fig. 2*D*). Meanwhile, the production of lactate and pyruvate was found to be significantly increased when hepatocytes treated with [U-^{13}C]glucose in the presence of palmitate compared with in the absence of palmitate. Subsequently, labeled lactate and pyruvate were mainly derived from [U-^{13}C]glucose (~90 and 85%, respectively) (Fig. 2, *D* and *E*). Together, these studies showed that palmitate oxidation leads to metabolic reprogramming, whereby fatty acid carbon is preferentially oxidized over glucose sources. This resulted in the fatty acid-derived carbon labeling a significant fraction of the acetyl-CoA pool during inflammation, while the pyruvate from glucose was mainly used to produced lactate. In this way, fatty acid-derived carbon becomes the dominant source of acetyl-CoA, rather than glucose, during the inflammatory stress response (Fig. 2*G*).

Inflammation exacerbates acetylation of mitochondrial proteins. The inventories of acetylated peptides detected in liver tissue were evaluated to gain further insights into the impact of LPS on the liver acetylome. The proteomic method employed was based on sensitive immunoaffinity purification using high-resolution LC-MS/MS to identify acetylated proteins and their modification sites in the liver (Fig. 3*A*). The acetyl peptides were identified with a 1% false discovery rate (FDR). Altogether, 726 lysine acetylation sites were identified in 382 protein groups, among which 511 sites in 286 proteins were quantified. A quantitative ratio >1.2 was considered to represent upregulation, while a ratio <0.83 was considered as downregulation (Supplemental Table S1; Supplemental Material for this article is available online at the Journal website). The amount of the differentially quantified sites and proteins are summarized in Fig. 3*B*. The mass error of all the identified peptides was verified. The distribution of mass error was ~0, and the majority was <0.02 Da, indicating that the MS data were satisfactory (Wang T, Yao W, Li J, He Q, Shao Y, Huang F, unpublished observations). Additionally, the length of most peptides was in the 8–20 range of tryptic peptides, indicating that the sample preparation reached the necessary standard (Wang T, Yao W, Li J, He Q, Shao Y, Huang F, unpublished observations).

The gene ontology (GO), domain, pathway, and subcellular localization were studied to further understand the function and feature of both identified and quantified proteins. The amount of identified proteins was added to that of the quantified proteins in each level 2 GO term. The results for both biological processes and molecular function showed that the largest group of acetylated proteins consists of enzymes associated with metabolism, accounting for 40 and 52% of the total acetylated proteins. Then, the quantifiable proteins were plotted for GO enrichment-based cluster analysis. Using Z-score transformed data, we performed a cluster analysis of acetyl peptides that differed in abundance by at least 1.5-fold (adjusted $P < 0.05$).

The quantifiable proteins were divided into four quantitative categories according to their LPS/control ratios: Q1 ($0 <$ LPS/control ≤ 0.67); Q2 ($0.67 <$ LPS/control ≤ 0.83); Q3 ($1.2 <$ LPS/control ≤ 1.5); and Q4 (>1.5 LPS/control). Enrichment-based cluster analysis of protein domains and Kyoto Encyclopedia of Genes and Genomes (KEGG) pathways showed that most of the upregulated acetylated proteins in the KEGG pathway are involved in butanoate metabolism, branched chain amino acid degradation, and peroxisome and fatty acid metabolism (Fig. 3*F*). Most of the upregulated acetylated proteins were found to be involved in NAD(P)binding and metallothionein domains (Fig. 3*F*). The results from GO enrichment-based cluster analysis indicated that most upregulated acetylation concentrates on glutathione transferase and transferase activities (Fig. 3*E*). Subcellular localization of the acetylated proteins showed that, among the upregulated proteins, 48% were distributed in the mitochondria, 26% were located in the cytoplasm, 15% in the nuclei, and 7% in the extracellular space (Fig. 3, *C* and *D*).

The amount of the quantifiable proteins in each subcellular localization was added. According to the results of subcellular localization classification, the upregulated acetyl peptides de-

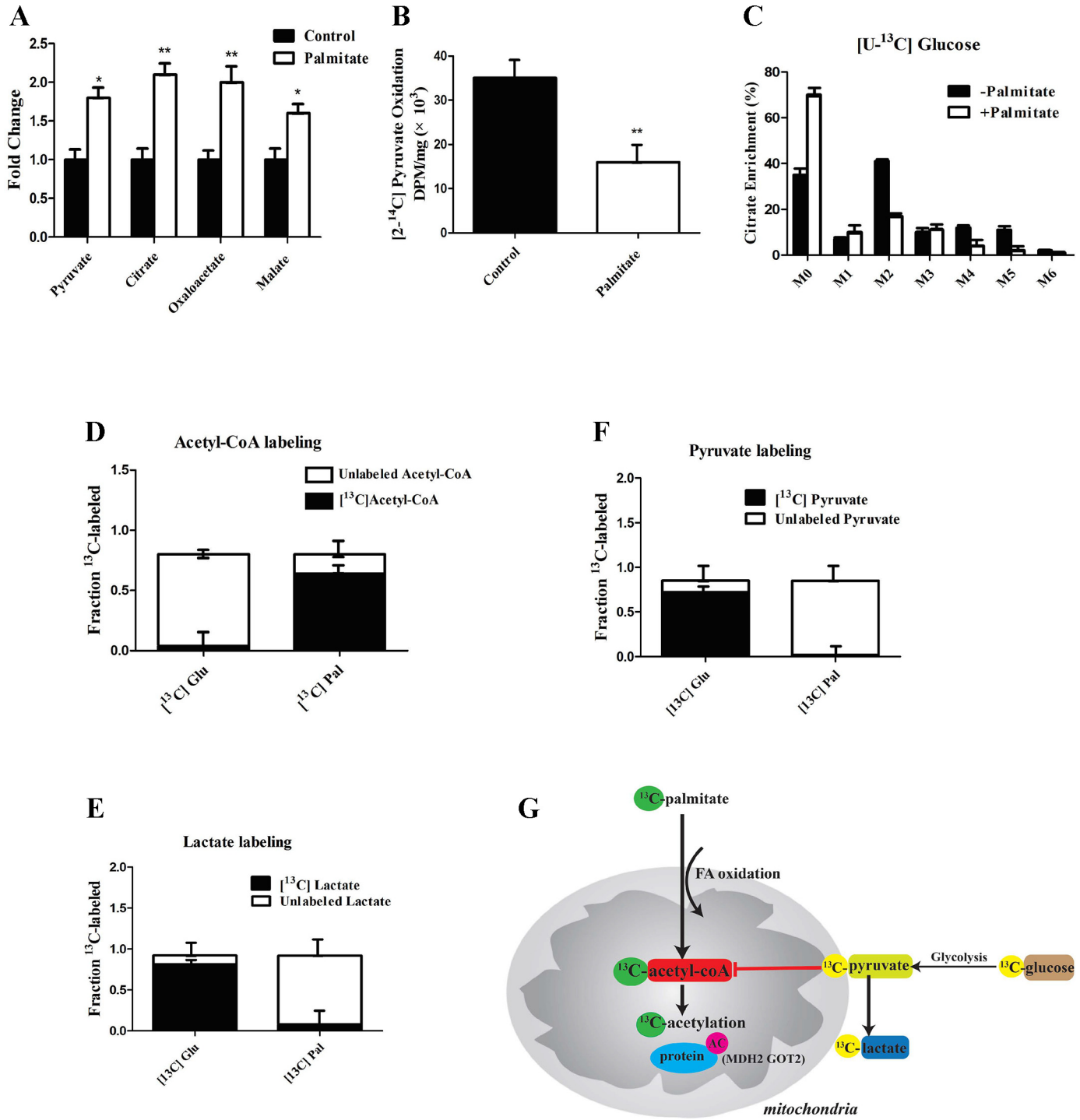

Fig. 2. Acetyl-CoA is mainly from fatty acid (FA) oxidation rather than pyruvate carboxylation in hepatocytes from LPS pigs. *A*: organic acid levels of hepatocytes isolated from LPS pigs treated in quadruplicate for 24 h with 2 mM palmitate (Pal) compared with control. Data are fold change over control (control indicates hepatocyte isolated from LPS pigs with no treatments). *B*: ^{14}C-labeled pyruvate oxidation in hepatocyte treated with or without palmitate in complete media for 24 h before capture and measurement of $^{14}CO_2$. Data are means ± SD; $n = 6$. $^*P < 0.05$, $^{**}P < 0.01$ from control group. *C*: mass isotopomer distribution of citrate from [U-^{13}C]glucose (Glu) in the presence or absence of unlabeled 2 mM octanoate. Error bars represent ± SD. *D–F*: acetyl-CoA, lactate, and pyruvate labeling pattern from hepatocyte treated with [U-^{13}C]-labeled substrates. Error bars represent ± SD. *G*: model showing the metabolic fates of [^{13}C]palmitate and [^{13}C]glucose. GOT2, mitochondrial glutamate oxaloacetate transaminase 2; MDH2, malate dehydrogenase 2.

tected in LPS-treated livers were derived from proteins that reside predominately in the mitochondrion, while the downregulated acetyl peptides were derived from those in the cytosol. This suggested that the size of the upregulated mitochondrion acetyl proteome, defined by the number of acetylation sites identified, was more than three times, which was a 300% increase relative to the downregulated acetyl proteome (Supplemental Table S1).

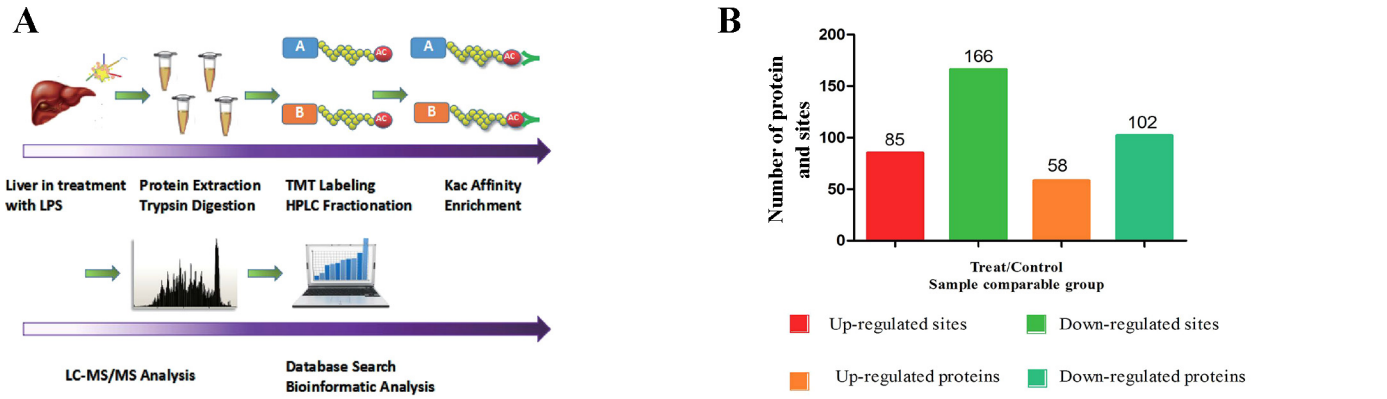

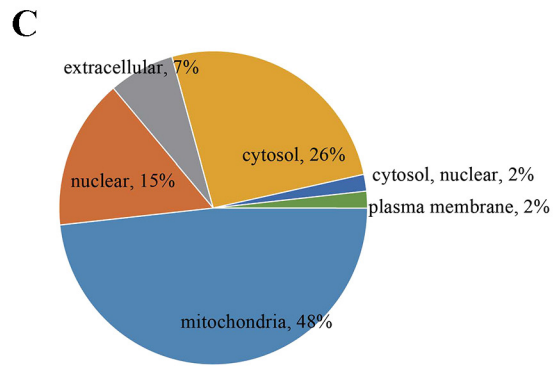

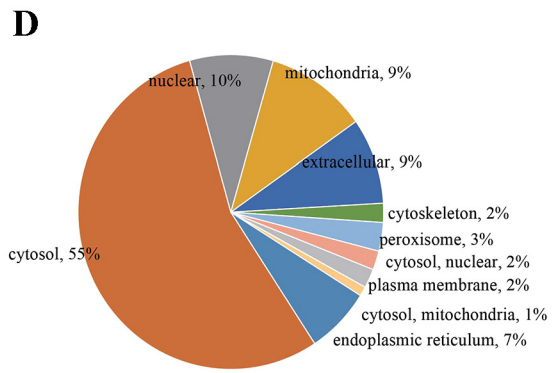

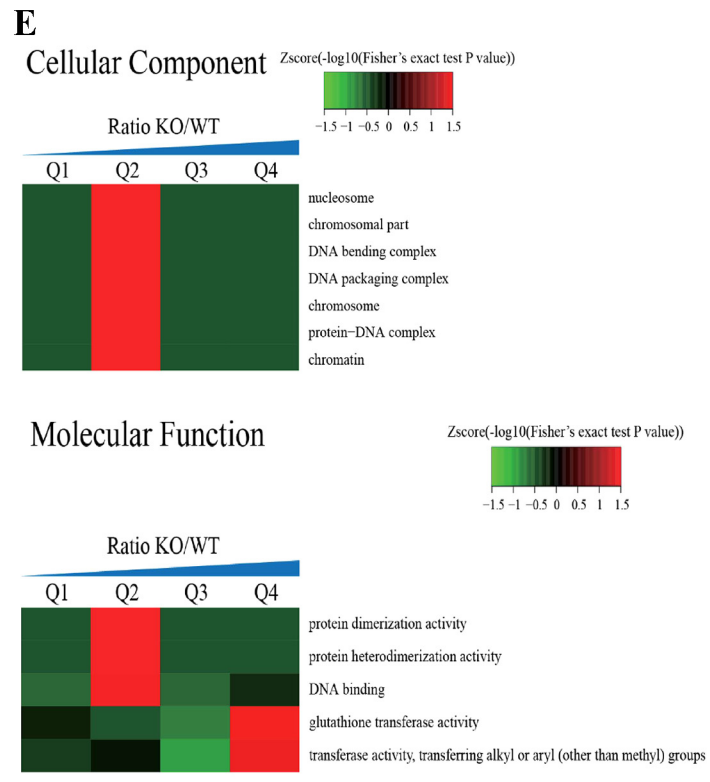

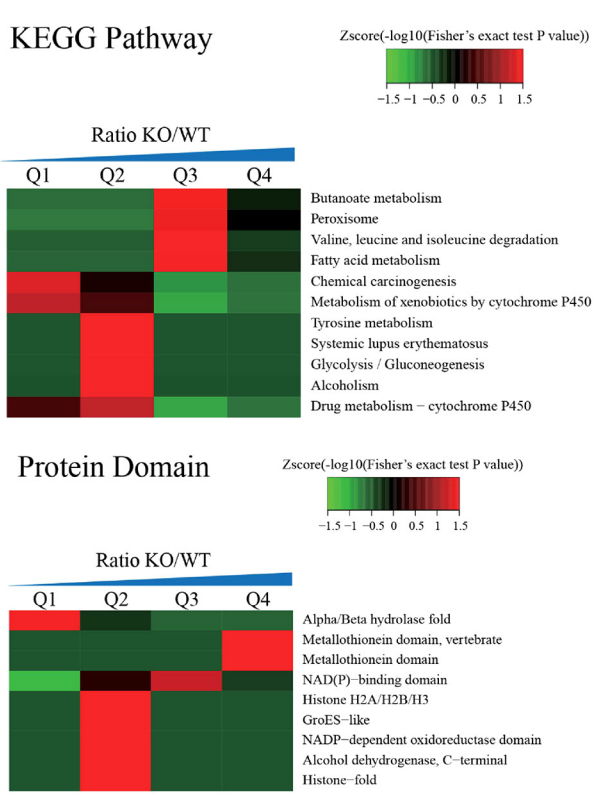

Most of the upregulated acetyl peptides in mitochondria were involved in metabolic processes such as those serving as enzymes in fatty acid metabolism (HADH and LCAD), the citrate cycle [isocitrate dehydrogenase (IDH2) and succinate dehydrogenase complex, subunit A (SDHA)], the urea cycle, pyruvate metabolism (PDH) and the metabolism of amino groups [carbamoyl-phosphate synthase 1 (CPS1), GOT2, MDH2, and ornithinecarbamoyl transferase (OTC)].

The level of acetylation of key glycolytic enzymes occurs mainly in the cytosol. Interestingly, mitochondrial MDH2 was acetylated at a high level compared with the control group (Supplemental Table S1). In addition, another mitochondrial metabolic enzyme, GOT2, which is also an important regulator in the carbon-nitrogen cycle, had increased acetylation levels (Supplemental Table S1). Moreover, in the cytoplasm, the acetylation level of the glycolytic enzyme LDHA was decreased (Supplemental Table S1). In this context, the enzymes involved in the carbon-nitrogen cycle and the metabolism of glucose and lipids were acetylated in both up- or downregulation, indicating that acetylation might play a major role in hepatic metabolic regulation during the inflammatory stress response, especially in the mitochondria.

Acetylation affects mitochondrial MDH2 and GOT2 enzymatic activity and enhances MAS activity. Both MDH2 and GOT2 were acetylated during the inflammatory stress response, and their acetylated lysine residues were identified (MDH2: K185, K301, K307, and K314; GOT2: K159, K184, and K404; Supplemental Table S1), which have been reported to affect the enzyme activity or binding (57, 59). Indeed, injection of LPS increased the MDH2 activity compared with the controls, but the activity of GOT2 was not significantly changed ($P < 0.01$, Fig. 4, *A* and *B*), consistent with the observation in previous studies (57). In addition, MAS activity in the liver of LPS-treated pigs was stimulated with respect to controls ($P < 0.001$, Fig. 4*C*). To verify that acetylation could affect the two enzymes and MAS activity, endogenous and ectopically expressed MDH2 and GOT2 activity were tested in Chang liver cells treated with TSA and NAM. As the inhibitor of deacetylase, TSA and NAM indeed increased ectopically expressed MDH2 and GOT2 acetylation levels (Fig. 4, *D* and *E*). TSA and NAM significantly increased the endogenous MDH2 activity but had no effect on GOT2 activity ($P < 0.001$, Fig. 4, *F* and *G*). Consistently, treatment with TSA and NAM activated the wild-type (WT) MDH2 but not the MDH2 4KR mutant, in which the four acetylated lysine residues were replaced with arginine in transfected HEK293T cells. While the activity of WT GOT2 and the 3KR mutant, in which the three acetylated lysine residues were replaced with arginine, were not changed ($P < 0.001$, Fig. 4, *F* and *G*). Furthermore, TSA and NAM activated MAS in WT MDH2 + WT GOT2 but not in the MDH2 4KR mutant + WT GOT2 or the GOT2 3KR mutant + WT MDH2 compared with the controls. Then, using the K-to-Q mutation of both MDH2 and GOT2, which was reported to abolish the positive charge and may act as a surrogate of acetylation, MAS was found to be reactivated ($P < 0.001$, Fig. 4*H*). This observation revealed that acetylation of MDH2 and GOT2 activated MAS and that it may be due to the previously reported observation that the acetylation of GOT2 at K159, K185, and K404 enhances its binding with MDH2 and MAS activity (57). Moreover, the in vitro deacetylation of immunopurified MDH2 and GOT2 by CobB deacetylase decreased MDH2 activity but had no effect on GOT2 activity; however, MDH2 deacetylation also decreased MAS activity, indicating that acetylation directly activates MDH2 and MAS but has no effects on GOT2 ($P < 0.01$, Fig. 4, *I* and *J*).

Acetyl-CoA from palmitate promotes MAS activity and glycolysis in primary hepatocytes. To test the ability of acetyl-CoA in the mitochondrial matrix to affect mitochondrial MDH2 and GOT2 via nonenzymatic acetylation, detergent-solubilized liver mitochondria were incubated at pH 7.8 with 5 mM acetyl-CoA, followed by enzyme activity assays. Mitochondrial MDH2 activity increased by 50% with this treatment, while GOT2 increased 15% ($P < 0.01$, Fig. 5*A*). With the use of an anti-acetyl lysine antibody, both MDH2 and GOT2 acetylation levels were found to be significantly increased in acetyl-CoA treatment compared with the control (Fig. 5*B*). Of note, MS analyses found the abundance of MDH2 and GOT2 lysine residues, which were identified in an in vivo experiment, were significantly increased, indicating that treatment of acetyl-CoA increased the lysine acetylation of MDH2 and GOT2 at certain sites and affected their enzyme activities.

Furthermore, a cell experiment was conducted to determine whether acetyl-CoA from fatty acid oxidation could promote MAS activity and glycolysis in response to inflammatory stress. Primary porcine hepatocytes isolated from LPS-injected pigs were treated with two concentrations (200 and 400 μM) of palmitate to induce a metabolic state in cells that is characterized by high fatty acid oxidation rates. To induce a decrease in fatty acid oxidation, hepatocytes were transfected with siRNAs of LCAD. After transfection, LCAD protein expression decreased by ~80% ($P < 0.01$, Fig. 5*C*), and the palmitate oxidation rate and hepatocyte level of acetyl-CoA were both significantly decreased compared with controls (hepatocyte from LPS-injected pigs) and the other groups. High concentrations of palmitate significantly increased the hepatocyte level of acetyl-CoA compared with the low concentrations of palmitate in the controls ($P < 0.01$, Fig. 5*K*).

Of note, the acetylation level of MDH2 and GOT2 was determined in cells treated with palmitate and LCAD-deficient hepatocytes. There was a large increase in acetylation both in MDH2 and GOT2 in hepatocytes with palmitate but not in LCAD-deficient hepatocytes with palmitate, while high concentrations of palmitate further increased MDH2 and GOT2 by

Fig. 3. Detectable acetyl-proteome in pig liver during inflammatory stress. *A*: schematic of the experimental workflow. *B*: the number of protein and sites of upregulated (red) proteins. The number of protein and sites of downregulated (green) proteins (treat vs. control). *C* and *D*: the subcellular location of upregulated and downregulated proteins (treat vs. control) and for the subcellular location of up- and downregulated proteins in other groups. *E* and *F*: heat maps obtained from gene onotology enrichment-based cluster analysis, and heat map obtained from enrichment-based cluster analysis of protein domains and KEGG pathways. The quantifiable proteins in the current study were divided into four quantitative categories according to their treat/control ratios: Q1 ($0 <$ ratio treat/control ≤ 0.667); Q2 ($0.67 <$ ratio treat/control ≤ 0.83); Q3 ($1.2 <$ ratio treat/control ≤ 1.5); and Q4 (ratio treat/control > 1.5). Then, the quantifiable proteins from the 4 categories were plotted for gene ontology enrichment-based cluster analysis. WT, wild type; KO, knockout; LC-MS/MS, liquid chromatography-mass spectrometry/mass spectrometry.

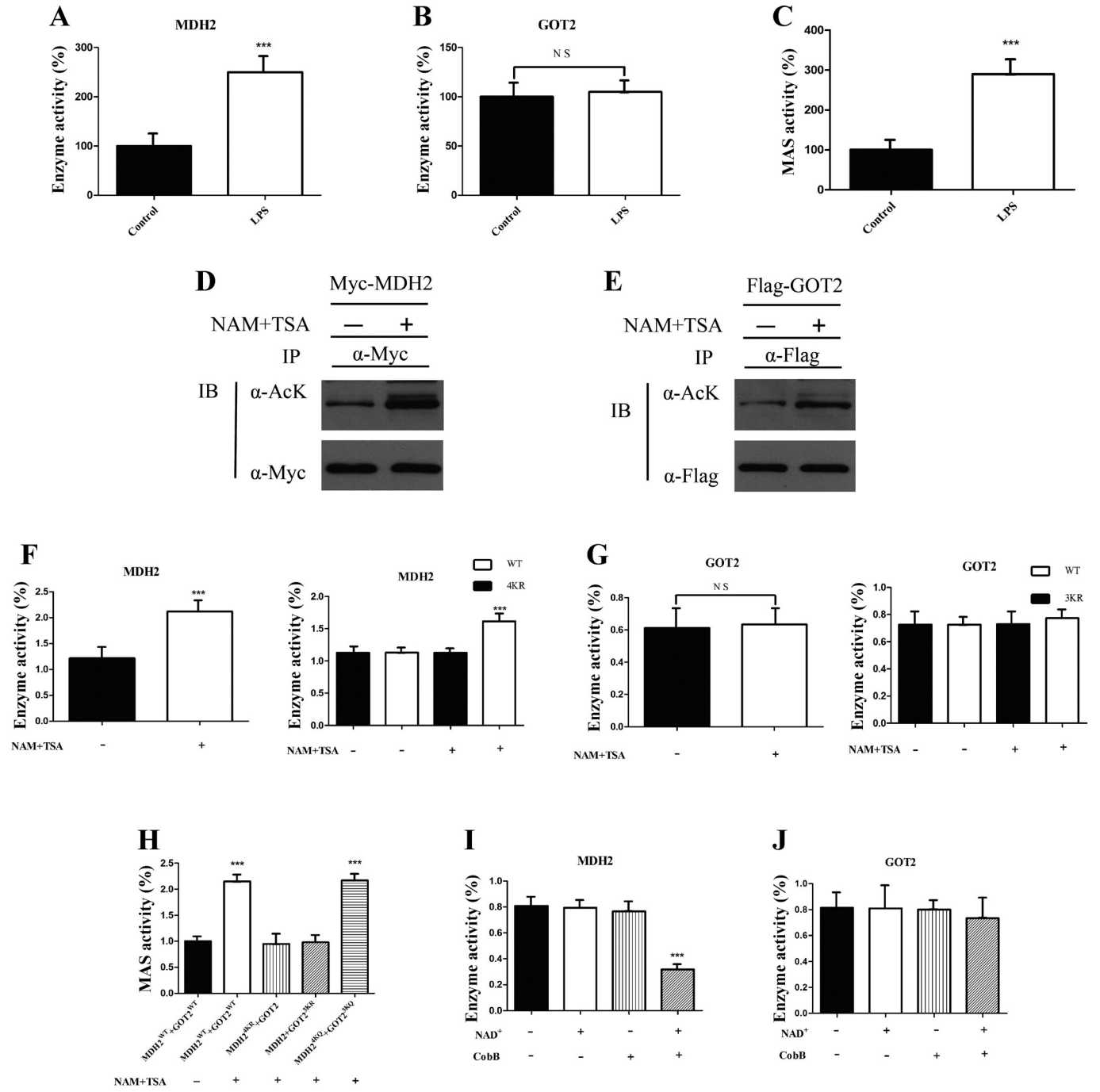

Fig. 4. Acetylation affects mitochondrial glutamate oxaloacetate transaminase 2 (GOT2) and malate dehydrogenase 2 (MDH2) enzyme activity and enhances the malate-aspartate shuttle (MAS) activity. *A–C*: MDH2, GOT2 enzyme activity, and MAS activity in the liver of LPS-treated pigs compare with controls. Data are means ± SD; $n = 6$. ***$P < 0.001$ from control group; NS, not significant for the indicated comparison. Liver tissue samples were collected from pigs after 7-h LPS/PBS (100 μg/kg body wt) injection. *D* and *E*: acetylation of MDH2 and GOT2. MDH2-Myc and Flag-GOT2 were expressed in HEK293T cells, and acetylation was determined by immunoblotting (IB). IP, immunoprecipitation. *F* and *G*: the activity of endogenous and ectopically expressed MDH2 and GOT2 from Chang and HEK293T cells, respectively. Data are means ± SD; $n = 6$. ***$P < 0.001$ from control group. *H*: the activity of MAS in HEK293T cells with or without nicotinamide (NAM) and trichostatin A (TSA) treatment. WT, wild type; KR, K-to-R mutation; KQ, K-to-Q mutation. Data are means ± SD; $n = 6$. ***$P < 0.001$ from control group. *I* and *J*: MDH2 and GOT2 enzyme activity. Immunoprecipitated MDH2 and GOT2 were incubated with or without CobB deacetylase. NAD, an essential cofactor for CobB, was omitted as a negative control. Data are means ± SD; $n = 6$. ***$P < 0.001$ from control group.

~50% ($P < 0.01$, Fig. 5*D*). MAS activity and the enzymatic activity of MDH2 and GOT2 were also measured. The MDH2 and MAS activities were significantly decreased in LCAD-deficient hepatocytes with palmitate compared with hepatocytes with palmitate and controls ($P < 0.01$, Fig. 5, *E* and *G*). In addition, the GOT2 activity was significantly decreased in LCAD-deficient hepatocytes with palmitate compared with hepatocytes with palmitate but did not significantly decrease it to the level of the controls ($P < 0.01$, Fig. 5*F*). Given that most acetylation occurs in the mitochondria and that SIRT3 is the

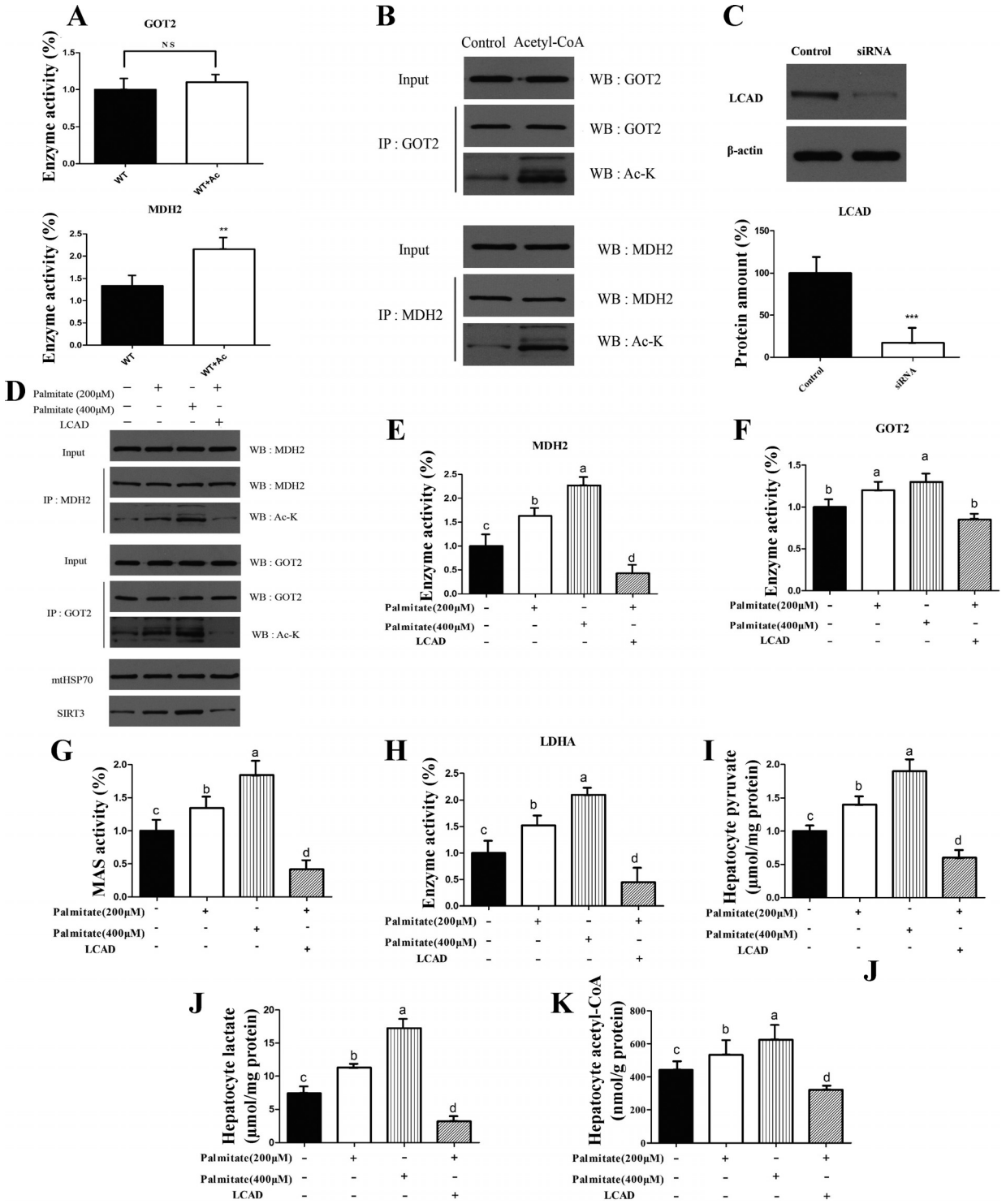

Fig. 5. Acetyl-CoA from palmitate promotes malate-aspartate NADH shuttle activity and glycolysis. *A*: activity of glutamate oxaloacetate transaminase 2 (GOT2) and malate dehydrogenase 2 (MDH2) in mitochondria treated with acetyl-CoA compared with untreated controls. Ac, treated with acetyl-CoA; WT control, wild type treated without acetyl-CoA. Data are means ± SD; $n = 6$. $^{**}P < 0.01$ from control group; NS, not significant for the indicated comparison. *B*: MDH2 and GOT2 acetylation levels in mitochondria treated with acetyl-CoA compared with untreated controls. *C*: long-chain fatty acid desaturase (LCAD) expression in primary porcine hepatocytes isolated from LPS- injected pigs after LCAD siRNA transfection. *D*: acetylation level of MDH2, GOT2, and SIRT3 in hepatocytes. *E–G*: activity of MDH2, GOT2, and malate-aspartate shuttle (MAS) in hepatocytes. Data are means ± SD; $n = 6$. $^{a,b,c,d}P < 0.001$, significantly different from each other group, respectively. *H–K*: lactate dehydrogenase A (LDHA) enzyme activity, pyruvate concentration (μmol/mg protein), lactate (μmol/mg protein), and acetyl-CoA content (nmol/g protein) in hepatocytes. Data are means ± SD; $n = 6$. $^{a,b,c,d}P < 0.001$, significantly different from each other group, respectively.

main mitochondrial deacetylase in the liver (28), this increased acetylation could also be explained by a decrease in the levels of SIRT3. Then, the SIRT3 expression was analyzed by Western blot analysis. SIRT3 levels in LCAD-deficient hepatocytes were not different from those of the controls, and palmitate slightly increased SIRT3 levels compared with LCAD-deficient hepatocytes ($P < 0.01$, Fig. 5*D*), indicating that the observed increase in MDH2 and GOT2 hyperacetylation cannot be explained by a decrease in SIRT3 expression.

Furthermore, increased treatment with palmitate significantly increased LDHA activity along with the lactate and pyruvate compared with the control ($P < 0.01$, Fig. 5, *H–J*). LCAD-deficient hepatocytes with palmitate significantly decreased LDHA activity along with the production of lactate and pyruvate compared with hepatocytes with palmitate and control ($P < 0.01$, Fig. 5, *H–J*).

DISCUSSION

Various inflammatory diseases are common complications of metabolic disorders such as obesity. Low- or high-grade systemic inflammation in adipose tissues or liver is an important etiologic factor in insulin resistance (50). LPS is an important element causing such metabolic inflammation, and it is the major virulence factor of most gram-negative bacteria that induces a series of immune reactions (42, 50). Additionally, the liver, regarded as the center of substance and energy metabolism, is one of the organs most easily targeted by LPS (50). Many studies of acute or chronic systemic inflammatory diseases now conclude that the inflammatory phase and immune effector responses depend on glycolysis and mitochondrial fatty acid oxidation as fuel sources (40). LPS-induced inflammation has been used to mimic the acute-phase response and analyze the mechanisms of inflammation (20, 31). In the present study, LPS infusion was used as a stressor to create an inflammatory stress model, finding that the processes of both glycolysis and fatty acid oxidation were accelerated. The breakdown of glucose for the generation of pyruvate, along with the increase in PK and GK enzyme activity and protein amount, suggested that glycolysis was promoted for energy production in response to inflammatory stress. Moreover, the results in vivo also showed that the enzyme activity of LCAD, HADH, and L-CPT-1, which play a central role in fatty acid oxidation in the liver, increased along with the plasma NEFA in the LPS-treated group. Of note, a previous study demonstrated that inflammation would cause adipose tissue lipolysis and increased levels of hepatic acetyl-CoA (41). In the current study, the content of the intermediate of fatty acid oxidation, acetyl-CoA, was indeed increased after LPS injection, indicating that NEFA oxidation was also activated in the liver of LPS-injected pigs. Thus these findings suggested that glycolysis and fatty acid oxidation were both increased in response to inflammatory stress in the liver of pigs.

Acetyl-CoA is a central metabolite that is involved in many metabolic transformations within the cell (7). For energy production, the generation of acetyl-CoA in the mitochondria is mainly supplied by glucose-derived pyruvate oxidative decarboxylation or lipid-derived fatty acid oxidation. It is well known that, in mammalian cells, glucose is oxidized to pyruvate and generates NADH through the glycolytic pathway and that there are two major pyruvate metabolic pathways. Pyruvate dehydrogenase can catalyze pyruvate to acetyl-CoA, which then enters the TCA cycle and is oxidized to NADH. Finally, NADH is oxidized and generates ATP to provide energy for cellular metabolism. Pyruvate can also be catalyzed by LDHA, which results in lactate production (56). In the present study, metabolite analysis of hepatic vein blood showed that the generation of lactate and the activity of the hepatic LDHA were increased after treatment with LPS, which indicates that the second pathway of pyruvate metabolism may be activated in LPS-injected pig liver. According to the results in vivo concerning fatty acid oxidation and hepatic acetyl-CoA, there is a possibility that the accumulation of acetyl-CoA is mainly due to fatty acid oxidation rather than pyruvate oxidative decarboxylation in response to inflammatory stress. To verify this hypothesis, this study further used ^{13}C-labeled palmitate and ^{13}C-labeled glucose to test which is the primary carbon source of acetyl-CoA during the inflammatory stress response. As expected, the percentage of ^{13}C-labeled palmitate-derived acetyl-CoA was considerably more than glucose, while the lactate levels were almost entirely from the ^{13}C-labeled glucose. Moreover, by examining the isotope labeling pattern of citrate, we found that fatty acid oxidation reduced the contribution of glucose to the TCA cycle. Together, these results give direct evidence to the hypothesis that hepatic accumulation of acetyl-CoA is mainly due to the fatty acid oxidation rather than pyruvate oxidative decarboxylation during the inflammatory stress response.

Glucose and fatty acid oxidation occur in the mitochondria, which integrates metabolic networks to maintain bioenergetic requirements. Functional studies have provided evidence that acetylation of certain lysine residues can affect mitochondrial protein interactions, function, and/or enzymatic activities (18, 22). In addition, a previous theory postulates that mitochondrial metabolism generates large amounts of acetyl-CoA, leading to the speculation that mitochondrial acetylation can occur nonenzymatically (10, 15, 33, 51). These findings suggest there is a link between the metabolic state of the cell and the level of mitochondrial protein acetylation. As LPS treatment activated hepatic fatty acid oxidation and lactate production while inhibiting glucose shuttling to the TCA cycle, there is a serious possibility that the reprogramming of these two nutrients may be due to mitochondrial acetyl-CoA-induced protein acetylation in response to inflammatory stress.

Mitochondrial protein hyperacetylation was confirmed by the acetylome analysis results. Quantitative lysine acetylome analysis showed that LPS resulted in 726 lysine acetylation sites in which 382 protein groups were identified and among which 511 sites in 286 different proteins were quantified. According to the results of the subcellular localization classification, the subset of upregulated acetyl peptides detected after LPS treatment were derived from proteins that reside predominately in the mitochondrion. Most of the upregulated mitochondrial acetyl peptides were involved in metabolic processes. For example, the enzyme acetylation levels of fatty acid metabolism (HADH and LCAD), the citrate cycle (IDH2 and SDHA), the urea cycle, the metabolism of amino groups (CPS1, GOT2, MDH2, and OTC), and pyruvate metabolism (PDH and LDHA) were shown to be differently affected.

According to these observations, the hepatic enzyme acetylation level was globally changed, and the phenomenon may be associated with metabolic dysfunction. Of the upregulated

acetyl peptides of the mitochondrion, MDH2 and GOT2 are two major mitochondrial enzymes in the MAS pathway that are known to be closely related to glycolysis and have increased levels of acetylation. MAS is one of the NADH shuttles largely known to mediate the transfer of the reducing equivalents of cytosolic NADH into the mitochondria and then maintain the glycolysis (52). Previous proteomic analyses using MS have identified several acetylated proteins, including GOT2 and MDH2. Moreover, MAS activity can be affected by GOT2 acetylation at lysine residues K159, K185, and K404 (57). Another study demonstrated that the acetylation of MDH2 at K185, K301, K307, and K314 might increase its activity, which may also in turn affect the activity of MAS (59). In the present study, LPS treatment increased hepatic MDH2 and MAS activity but had no effect on GOT2 activity. Acetylome analysis also identified all the lysine residues that were previously reported to be acetylated in GOT2 and MDH2. With the use of the same method, this study verified that the acetylation of MDH2 at these sites increased MDH2 activity, while the acetylation of GOT2 did not, which was consistent with the results in vivo.

SIRT3 is known to be the major mitochondrial deacetylase and a general regulator of protein hyperacetylation (28). As GOT2 and MDH2 were localized in the mitochondria and the acetylation status of GOT2 was previously proved to be affected by SIRT3, there is a possibility that the hyperacetylation of MDH2 and GOT2 may be due to the decrease in SIRT3 levels. Instead, our in vivo results showed that LPS treatment slightly increased SIRT3 protein levels, thus seeming to rule out the possibility that reduced SIRT3 levels promotes MDH2/GOT2 hyperacetylation. We then tested if the acetylation of MDH2 and GOT2 was due to acetyl-CoA. Interestingly, treatment with acetyl-CoA directly increased MDH2 activity and the acetylation level of MDH2 and GOT2. These results indicated that acetyl-CoA-induced acetylation of MDH2 and GOT2 affects the enzymatic activity of MDH2. As hepatic glycolysis has been accelerated in response to inflammatory stress, it seems to be regulated by lysine acetylation of these two enzymes, and this PTM may be regulated via generation of acetyl-CoA by fatty acid oxidation.

To test the hypothesis, this study examined the inflammatory stress response in hepatocytes isolated from LPS-injected pigs. Treatment with different concentrations of palmitate directly increased the acetylation level of MDH2 and GOT2, the activity of MAS, and the production of acetyl-CoA, pyruvate, lactate, and LDHA. However, the deficiency of LCAD treatment inhibited this phenomenon. In addition, the SIRT3 level was not significantly affected by treatment with palmitate or LCAD-deficient hepatocytes, which was consistent with the observation in vivo. These results further verified that the acetylation level of MDH2 and GOT2 was directly linked to increased fatty acid oxidation flux. Altogether, these observations showed that fatty acid oxidation-induced acetyl-CoA stimulated MAS activity and glycolysis via a nonenzymatic acetylation mechanism.

In conclusion, the results presented in the current study demonstrate that the generation of acetyl-CoA through hepatic fatty acid oxidation is critical for the regulation of hepatic mitochondrial nonenzymatic acetylation during inflammation in vivo. Additionally, nonenzymatic acetylation stimulated MAS activity and maintained glycolysis during the inflammatory stress response. As fatty acid oxidation directly repressed the contribution of glucose to TCA cycle, increased glucose utilization mainly contributed to lactate production during inflammation. In other words, our work showed fatty acid oxidation-induced hepatic mitochondrial protein acetylation as a novel process for modulating inflammatory-metabolic reprogramming of glucose. The reprogramming of the metabolic pathways in hepatocytes and acetyl-CoA-induced nonenzymatic acetylation could have relevance in the pathogenesis of inflammatory and metabolic diseases and could provide novel therapeutic strategies.

ACKNOWLEDGMENTS

We thank members of our laboratory, Weilei Yao, Ji Li, Qiongyu He, and Yafei Shao for helpful and constructive advice.

GRANTS

This work was supported by the National Natural Science Foundation of China Grant 31572409, National Basic Research Program of China Grant 2013CB127304, and National Key Research and Development Program Grant 2016YFD0500506.

DISCLOSURES

No conflicts of interest, financial or otherwise, are declared by the authors.

AUTHOR CONTRIBUTIONS

T.W. and F.H. conceived and designed research; T.W., W.Y., J.L., Q.H., and Y.S. performed experiments; T.W. and W.Y. analyzed data; T.W., W.Y., and J.L. interpreted results of experiments; T.W. prepared figures; T.W. and W.Y. drafted manuscript; T.W. and W.Y. edited and revised the manuscript; T.W., W.Y., Q.H., Y.S., and F.H. approved final version of manuscript.

REFERENCES

1. **Ahn WS, Antoniewicz MR.** Metabolic flux analysis of CHO cells at growth and non-growth phases using isotopic tracers and mass spectrometry. *Metab Eng* 13: 598–609, 2011. doi:10.1016/j.ymben.2011.07.002.
2. **Alcaín FJ, Villalba JM.** Sirtuin activators. *Expert Opin Ther Pat* 19: 403–414, 2009. doi:10.1517/13543770902762893.
3. **Alcaín FJ, Villalba JM.** Sirtuin inhibitors. *Expert Opin Ther Pat* 19: 283–294, 2009. doi:10.1517/13543770902755111.
4. **Bechmann LP, Hannivoort RA, Gerken G, Hotamisligil GS, Trauner M, Canbay A.** The interaction of hepatic lipid and glucose metabolism in liver diseases. *J Hepatol* 56: 952–964, 2012. doi:10.1016/j.jhep.2011.08.025.
5. **Berry KE, Lineweaver H.** *Objective Methodology to Differentiate Between Fresh and Frozen-and-Thawed Meats*. http://www.dtic.mil/dtic/tr/fulltext/u2/a026237.pdf. [1975].
6. **Biswas SK, Mantovani A.** Orchestration of metabolism by macrophages. *Cell Metab* 15: 432–437, 2012. doi:10.1016/j.cmet.2011.11.013.
7. **Cai L, Tu BP.** On acetyl-CoA as a gauge of cellular metabolic state. *Cold Spring Harb Symp Quant Biol* 76: 195–202, 2011. doi:10.1101/sqb.2011.76.010769.
8. **Chen L, Magliano DJ, Zimmet PZ.** The worldwide epidemiology of type 2 diabetes mellitus–present and future perspectives. *Nat Rev Endocrinol* 8: 228–236, 2012. doi:10.1038/nrendo.2011.183.
9. **Close P, Creppe C, Gillard M, Ladang A, Chapelle JP, Nguyen L, Chariot A.** The emerging role of lysine acetylation of non-nuclear proteins. *Cell Mol Life Sci* 67: 1255–1264, 2010. doi:10.1007/s00018-009-0252-7.

9a. **Contreras L, Satrustegui J.** Calcium signaling in brain mitochondria: interplay of malate aspartate NADH shuttle and calcium uniporter/mitochondrial dehydrogenase pathways. *J Biol Chem* 284: 7091–7099, 2009. doi:10.1074/jbc.M808066200.

10. **Davies MN, Kjalarsdottir L, Thompson JW, Dubois LG, Stevens RD, Ilkayeva OR, Brosnan MJ, Rolph TP, Grimsrud PA, Muoio DM.** The acetyl group buffering action of carnitine acetyltransferase offsets macronutrient-induced lysine acetylation of mitochondrial proteins. *Cell Reports* 14: 243–254, 2016. doi:10.1016/j.celrep.2015.12.030.

11. **Dittenhafer-Reed KE, Richards AL, Fan J, Smallegan MJ, Fotuhi Siahpirani A, Kemmerer ZA, Prolla TA, Roy S, Coon JJ, Denu JM.** SIRT3 mediates multi-tissue coupling for metabolic fuel switching. *Cell Metab* 21: 637–646, 2015. doi:10.1016/j.cmet.2015.03.007.
12. **Egnatchik RA, Leamy AK, Jacobson DA, Shiota M, Young JD.** ER calcium release promotes mitochondrial dysfunction and hepatic cell lipotoxicity in response to palmitate overload. *Mol Metab* 3: 544–553, 2014. doi:10.1016/j.molmet.2014.05.004.
13. **Frerman FE, Goodman SI.** Fluorometric assay of acyl-CoA dehydrogenases in normal and mutant human fibroblasts. *Biochem Med* 33: 38–44, 1985. doi:10.1016/0006-2944(85)90124-3.
15. **Ghanta S, Grossmann RE, Brenner C.** Mitochondrial protein acetylation as a cell-intrinsic, evolutionary driver of fat storage: chemical and metabolic logic of acetyl-lysine modifications. *Crit Rev Biochem Mol Biol* 48: 561–574, 2013. doi:10.3109/10409238.2013.838204.
16. **Gradilone SA, Carreras FI, Lehmann GL, Marinelli RA.** Phosphoinositide 3-kinase is involved in the glucagon-induced translocation of aquaporin-8 to hepatocyte plasma membrane. *Biol Cell* 97: 831–836, 2005. doi:10.1042/BC20040115.

16a. **Gronemeyer T, Wiese S, Ofman R, Bunse C, Pawlas M, Hayen H, Eisenacher M, Stephan C, Meyer HE, Waterham HR, Erdmann R, Wanders RJ, Warscheid B.** The proteome of human liver peroxisomes: identification of five new peroxisomal constituents by a label-free quantitative proteomics survey. *PLoS One* 8: e57395, 2013. [Erratum in *PLoS One* 8: 10.1371/annotation/3552e5c7-88d1-42c5-844d-4c2f2d722533, 2013]. doi:10.1371/journal.pone.0057395.

17. **Hebert AS, Dittenhafer-Reed KE, Yu W, Bailey DJ, Selen ES, Boersma MD, Carson JJ, Tonelli M, Balloon AJ, Higbee AJ, Westphall MS, Pagliarini DJ, Prolla TA, Assadi-Porter F, Roy S, Denu JM, Coon JJ.** Calorie restriction and SIRT3 trigger global reprogramming of the mitochondrial protein acetylome. *Mol Cell* 49: 186–199, 2013. doi:10.1016/j.molcel.2012.10.024.
18. **Hirschey MD, Shimazu T, Jing E, Grueter CA, Collins AM, Aouizerat B, Stančáková A, Goetzman E, Lam MM, Schwer B, Stevens RD, Muehlbauer MJ, Kakar S, Bass NM, Kuusisto J, Laakso M, Alt FW, Newgard CB, Farese RV Jr, Kahn CR, Verdin E.** SIRT3 deficiency and mitochondrial protein hyperacetylation accelerate the development of the metabolic syndrome. *Mol Cell* 44: 177–190, 2011. doi:10.1016/j.molcel.2011.07.019.
19. **Hue L, Taegtmeyer H.** The Randle cycle revisited: a new head for an old hat. *Am J Physiol Endocrinol Metab* 297: E578–E591, 2009. doi:10.1152/ajpendo.00093.2009.
20. **Imam F, Al-Harbi NO, Al-Harbi MM, Ansari MA, Zoheir KM, Iqbal M, Anwer MK, Al Hoshani AR, Attia SM, Ahmad SF.** Diosmin downregulates the expression of T cell receptors, pro-inflammatory cytokines and NF-κB activation against LPS-induced acute lung injury in mice. *Pharmacol Res* 102: 1–11, 2015. doi:10.1016/j.phrs.2015.09.001.
21. **Jensen MV, Joseph JW, Ilkayeva O, Burgess S, Lu D, Ronnebaum SM, Odegaard M, Becker TC, Sherry AD, Newgard CB.** Compensatory responses to pyruvate carboxylase suppression in islet beta-cells. Preservation of glucose-stimulated insulin secretion. *J Biol Chem* 281: 22342–22351, 2006. doi:10.1074/jbc.M604350200.
22. **Jing E, Emanuelli B, Hirschey MD, Boucher J, Lee KY, Lombard D, Verdin EM, Kahn CR.** Sirtuin-3 (Sirt3) regulates skeletal muscle metabolism and insulin signaling via altered mitochondrial oxidation and reactive oxygen species production. *Proc Natl Acad Sci USA* 108: 14608–14613, 2011. doi:10.1073/pnas.1111308108.
23. **Kendrick AA, Choudhury M, Rahman SM, McCurdy CE, Friederich M, Van Hove JL, Watson PA, Birdsey N, Bao J, Gius D, Sack MN, Jing E, Kahn CR, Friedman JE, Jonscher KR.** Fatty liver is associated with reduced SIRT3 activity and mitochondrial protein hyperacetylation. *Biochem J* 433: 505–514, 2011. doi:10.1042/BJ20100791.
24. **Krawczyk CM, Holowka T, Sun J, Blagih J, Amiel E, DeBerardinis RJ, Cross JR, Jung E, Thompson CB, Jones RG, Pearce EJ.** Toll-like receptor-induced changes in glycolytic metabolism regulate dendritic cell activation. *Blood* 115: 4742–4749, 2010. doi:10.1182/blood-2009-10-249540.
25. **Lavu S, Boss O, Elliott PJ, Lambert PD.** Sirtuins–novel therapeutic targets to treat age-associated diseases. *Nat Rev Drug Discov* 7: 841–853, 2008 [Erratum in *Nat Rev Drug Discov* 8: 516, 2009]. doi:10.1038/nrd2665.
26. **Leighty RW, Antoniewicz MR.** COMPLETE-MFA: complementary parallel labeling experiments technique for metabolic flux analysis. *Metab Eng* 20: 49–55, 2013. doi:10.1016/j.ymben.2013.08.006.
27. **Li L, Zhang P, Bao Z, Wang T, Liu S, Huang F.** PGC-1α promotes ureagenesis in mouse periportal hepatocytes through SIRT3 and SIRT5 in response to glucagon. *Sci Rep* 6: 24156, 2016. doi:10.1038/srep24156.
28. **Lombard DB, Alt FW, Cheng HL, Bunkenborg J, Streeper RS, Mostoslavsky R, Kim J, Yancopoulos G, Valenzuela D, Murphy A, Yang Y, Chen Y, Hirschey MD, Bronson RT, Haigis M, Guarente LP, Farese RV Jr, Weissman S, Verdin E, Schwer B.** Mammalian Sir2 homolog SIRT3 regulates global mitochondrial lysine acetylation. *Mol Cell Biol* 27: 8807–8814, 2007. doi:10.1128/MCB.01636-07.
29. **Lowell BB, Shulman GI.** Mitochondrial dysfunction and type 2 diabetes. *Science* 307: 384–387, 2005. doi:10.1126/science.1104343.
30. **Magnes C, Sinner FM, Regittnig W, Pieber TR.** LC/MS/MS method for quantitative determination of long-chain fatty acyl-CoAs. *Anal Chem* 77: 2889–2894, 2005. doi:10.1021/ac048314i.
31. **Masaki T, Chiba S, Tatsukawa H, Yasuda T, Noguchi H, Seike M, Yoshimatsu H.** Adiponectin protects LPS-induced liver injury through modulation of TNF-α in KK-Ay obese mice. *Hepatology* 40: 177–184, 2004. doi:10.1002/hep.20282.
32. **Mayers RM, Butlin RJ, Kilgour E, Leighton B, Martin D, Myatt J, Orme JP, Holloway BR.** AZD7545, a novel inhibitor of pyruvate dehydrogenase kinase 2 (PDHK2), activates pyruvate dehydrogenase in vivo and improves blood glucose control in obese (fa/fa) Zucker rats. *Biochem Soc Trans* 31: 1165–1167, 2003. doi:10.1042/bst0311165.
33. **McDonnell E, Crown SB, Fox DB, Kitir B, Ilkayeva OR, Olsen CA, Grimsrud PA, Hirschey MD.** Lipids reprogram metabolism to become a major carbon source for histone acetylation. *Cell Reports* 17: 1463–1472, 2016. doi:10.1016/j.celrep.2016.10.012.
34. **McGarry JD, Foster DW.** Regulation of hepatic fatty acid oxidation and ketone body production. *Annu Rev Biochem* 49: 395–420, 1980. doi:10.1146/annurev.bi.49.070180.002143.
35. **McGarry JD, Mills SE, Long CS, Foster DW.** Observations on the affinity for carnitine, and malonyl-CoA sensitivity, of carnitine palmitoyltransferase I in animal and human tissues. Demonstration of the presence of malonyl-CoA in non-hepatic tissues of the rat. *Biochem J* 214: 21–28, 1983. doi:10.1042/bj2140021.
36. **Menazza S, Wong R, Nguyen T, Wang G, Gucek M, Murphy E.** CypD(-/-) hearts have altered levels of proteins involved in Krebs cycle, branch chain amino acid degradation and pyruvate metabolism. *J Mol Cell Cardiol* 56: 81–90, 2013. doi:10.1016/j.yjmcc.2012.12.004.
37. **Minkler PE, Kerner J, Ingalls ST, Hoppel CL.** Novel isolation procedure for short-, medium-, and long-chain acyl-coenzyme A esters from tissue. *Anal Biochem* 376: 275–276, 2008. doi:10.1016/j.ab.2008.02.022.
38. **Newman JC, He W, Verdin E.** Mitochondrial protein acylation and intermediary metabolism: regulation by sirtuins and implications for metabolic disease. *J Biol Chem* 287: 42436–42443, 2012. doi:10.1074/jbc.R112.404863.
39. **O'Neill LA, Hardie DG.** Metabolism of inflammation limited by AMPK and pseudo-starvation. *Nature* 493: 346–355, 2013. doi:10.1038/nature11862.
40. **Palsson-McDermott EM, O'Neill LAJ.** The Warburg effect then and now: from cancer to inflammatory diseases. *BioEssays* 35: 965–973, 2013. doi:10.1002/bies.201300084.
41. **Perry RJ, Camporez JG, Kursawe R, Titchenell PM, Zhang D, Perry CJ, Jurczak MJ, Abudukadier A, Han MS, Zhang XM, Ruan HB, Yang X, Caprio S, Kaech SM, Sul HS, Birnbaum MJ, Davis RJ, Cline GW, Petersen KF, Shulman GI.** Hepatic acetyl CoA links adipose tissue inflammation to hepatic insulin resistance and type 2 diabetes. *Cell* 160: 745–758, 2015. doi:10.1016/j.cell.2015.01.012.
42. **Plaizier JC, Krause DO, Gozho GN, McBride BW.** Subacute ruminal acidosis in dairy cows: the physiological causes, incidence and consequences. *Vet J* 176: 21–31, 2008. doi:10.1016/j.tvjl.2007.12.016.
43. **Popov VN, Volvenkin SV, Kosmatykh TA, Suad A, Schnarrenberger C, Eprintcev AT.** Induction of a peroxisomal malate dehydrogenase isoform in liver of starved rats. *Biochemistry (Mosc)* 66: 496–501, 2001. doi:10.1023/A:1010298516534.
44. **Pougovkina O, te Brinke H, Ofman R, van Cruchten AG, Kulik W, Wanders RJ, Houten SM, de Boer VC.** Mitochondrial protein acetylation is driven by acetyl-CoA from fatty acid oxidation. *Hum Mol Genet* 23: 3513–3522, 2014. doi:10.1093/hmg/ddu059.
46. **Randle PJ, Garland PB, Hales CN, Newsholme EA.** The glucose fatty-acid cycle. Its role in insulin sensitivity and the metabolic disturbances of diabetes mellitus. *Lancet* 281: 785–789, 1963. doi:10.1016/S0140-6736(63)91500-9.
47. **Rardin MJ, Newman JC, Held JM, Cusack MP, Sorensen DJ, Li B, Schilling B, Mooney SD, Kahn CR, Verdin E, Gibson BW.** Label-free

quantitative proteomics of the lysine acetylome in mitochondria identifies substrates of SIRT3 in metabolic pathways. *Proc Natl Acad Sci USA* 110: 6601–6606, 2013. doi:10.1073/pnas.1302961110.

48. **Soria LR, Marrone J, Molinas SM, Lehmann GL, Calamita G, Marinelli RA.** Lipopolysaccharide impairs hepatocyte ureagenesis from ammonia: involvement of mitochondrial aquaporin-8. *FEBS Lett* 588: 1686–1691, 2014. doi:10.1016/j.febslet.2014.03.012.
49. **Still AJ, Floyd BJ, Hebert AS, Bingman CA, Carson JJ, Gunderson DR, Dolan BK, Grimsrud PA, Dittenhafer-Reed KE, Stapleton DS, Keller MP, Westphall MS, Denu JM, Attie AD, Coon JJ, Pagliarini DJ.** Quantification of mitochondrial acetylation dynamics highlights prominent sites of metabolic regulation. *J Biol Chem* 288: 26209–26219, 2013. doi:10.1074/jbc.M113.483396.
50. **Su GL.** Lipopolysaccharides in liver injury: molecular mechanisms of Kupffer cell activation. *Am J Physiol Gastrointest Liver Physiol* 283: G256–G265, 2002. doi:10.1152/ajpgi.00550.2001.
51. **Wagner GR, Payne RM.** Widespread and enzyme-independent Nε-acetylation and Nε-succinylation of proteins in the chemical conditions of the mitochondrial matrix. *J Biol Chem* 288: 29036–29045, 2013. doi:10.1074/jbc.M113.486753.
52. **Wang C, Chen H, Zhang M, Zhang J, Wei X, Ying W.** Malate-aspartate shuttle inhibitor aminooxyacetic acid leads to decreased intracellular ATP levels and altered cell cycle of C6 glioma cells by inhibiting glycolysis. *Cancer Lett* 378: 1–7, 2016. doi:10.1016/j.canlet.2016.05.001.
53. **Wang R, Green DR.** Metabolic checkpoints in activated T cells. *Nat Immunol* 13: 907–915, 2012. doi:10.1038/ni.2386.
54. **Wellen KE, Hotamisligil GS.** Inflammation, stress, and diabetes. *J Clin Invest* 115: 1111–1119, 2005. doi:10.1172/JCI25102.
55. **Wen H, Ting JP, O'Neill LA.** A role for the NLRP3 inflammasome in metabolic diseases–did Warburg miss inflammation? *Nat Immunol* 13: 352–357, 2012. doi:10.1038/ni.2228.
56. **Xia Z, Zhuang Y, Yi X.** Stable over-expression of the human malate-aspartate NADH shuttle member Aralar I in PK15 cells improves energy metabolism and enhances proliferation of porcine circovirus-2. *RSC Advances* 6: 61268–61277, 2016. doi:10.1039/C6RA06343H.
57. **Yang H, Zhou L, Shi Q, Zhao Y, Lin H, Zhang M, Zhao S, Yang Y, Ling ZQ, Guan KL, Xiong Y, Ye D.** SIRT3-dependent GOT2 acetylation status affects the malate-aspartate NADH shuttle activity and pancreatic tumor growth. *EMBO J* 34: 1110–1125, 2015. doi:10.15252/embj.201591041.
58. **Yang L, Xie M, Yang M, Yu Y, Zhu S, Hou W, Kang R, Lotze MT, Billiar TR, Wang H, Cao L, Tang D.** PKM2 regulates the Warburg effect and promotes HMGB1 release in sepsis. *Nat Commun* 5: 4436, 2014. doi:10.1038/ncomms5436.
59. **Zhao S, Xu W, Jiang W, Yu W, Lin Y, Zhang T, Yao J, Zhou L, Zeng Y, Li H, Li Y, Shi J, An W, Hancock SM, He F, Qin L, Chin J, Yang P, Chen X, Lei Q, Xiong Y, Guan KL.** Regulation of cellular metabolism by protein lysine acetylation. *Science* 327: 1000–1004, 2010. doi:10.1126/science.1179689.